Toward Continuum Robot Tentacles for Lung Interventions: Exploring Folding Support Disks

Margaret Rox[1], Daniel S. Esser[1], Mariana E. Smith[1], Tayfun Efe Ertop[1], Maxwell Emerson[1], Fabien Maldonado[2], Erin A. Gillaspie[2], Alan Kuntz[3], and Robert J. Webster III[1,2]

***Abstract*—Toward the future goal of creating a lung surgery system featuring multiple tentacle-like robots, we present a new folding concept for continuum robots that enables them to squeeze through openings smaller than the robot's nominal diameter (e.g., the narrow space between adjacent ribs). This is facilitated by making the disks along the robot's backbone foldable. We also demonstrate that such a robot can feature not only straight, but also curved tendon routing paths, thereby achieving a diverse family of conformations. We find that the foldable robot performs comparably, from a kinematic perspective, to an identical non-folding continuum robot at varying deployment lengths. This work paves the way for future applications with a continuum robot that can fold and fit through smaller openings, with the potential to reduce invasiveness during surgical tasks.**

***Index Terms*—Surgical Robotics: Laparoscopy, Soft Robot Materials and Design**

I. Introduction

MORE people die from lung cancer each year than from any other kind of cancer [1]. Surgical removal of tumors is the most effective treatment [2], [3], but open surgery is invasive and painful [4]. Video-Assisted Thoracoscopic Surgery (VATS), where rod-like instruments are inserted through the ribs is less invasive and offers lower mortality, shorter hospitalization, and faster recovery times than open surgery [5]. However, one third of all VATS patients face chronic pain which is believed to come from the tilting of the rod-like tools against the intercostal nerves around the ribs, leading to extended pain after surgery [4], [6]. Our long-term goal is to create a robotic system for lung surgery like that shown in Fig. 1 that will reduce the pressure applied to intercostal nerves, thereby reducing postoperative pain. Such a system may also have the potential to provide enhanced dexterity in lung surgery compared to laparoscopy, but this remains to be proven in future studies. As a first step, in this paper we explore ways to make continuum robots change their cross-sectional dimensions to fit through constrained entrances to surgical workspaces.

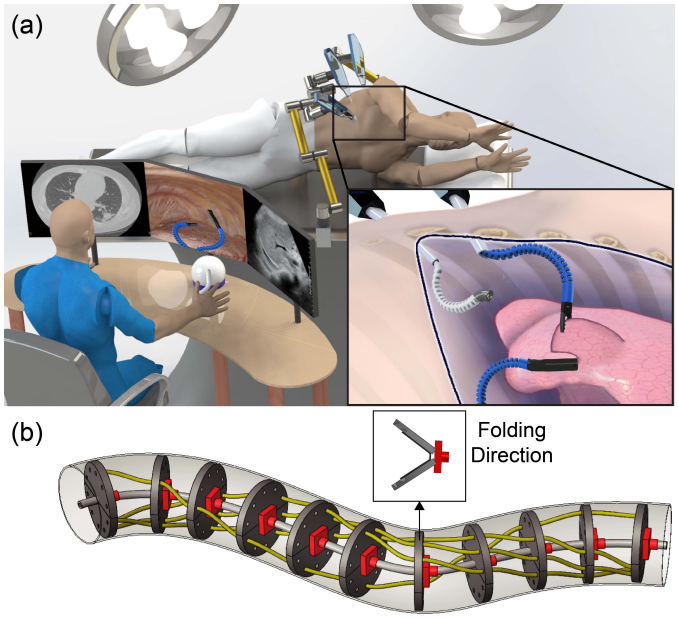

Fig. 1: Conceptual rendering of a multi-port continuum robot system for lung surgery. (a) Robotic system concept. (b) Close view of the new tendon arm concept, with inset showing folding.

Continuum robots are rod-like elastic robots that have been adapted to a variety of uses in medicine [7]–[9]. Tendon-actuated continuum robots usually consist of a central, flexible backbone and evenly spaced disks through which tendons pass. Typically, these robots are made with a circular cross-section and feature round disks to support tendons. It has also been shown that curved tendon paths can be beneficially used in these robots to create more complex curves (see Fig. 1b), or to adjust the robot's workspace [10]–[12]. In this paper, we explore how a device of this type might reduce its dimensions by employing passively foldable disks. We show that this folding concept enables the robot to pass through an opening that is narrower than the robot's initial diameter (see Fig. 2 for examples of this concept), which is well suited for squeezing

Manuscript received: October 26, 2022; Revised: February 11, 2023; Accepted: March 22, 2023. This paper was recommended for publication by Editor Pietro Valdastri upon evaluation of the Associate Editor and Reviewers' comments. This material is based upon work supported in part by the National Institutes of Health under NIBIB training grant T32EB021937 and in part by the National Science Foundation under grant numbers 2133027 and 1935278. Any opinions, findings, and conclusions or recommendations expressed in this material are those of the authors and do not necessarily reflect the views of the NIH or the NSF.

[1]Margaret Rox, Daniel S. Esser, Maxwell Emerson, Tayfun Efe Ertop, Mariana E. Smith, and Robert J. Webster III are with the Department of Mechanical Engineering, Vanderbilt University, Nashville, TN, 37203. (email: margaret.rox, robert.webster@vanderbilt.edu)

[2]Fabien Maldonado, Erin A. Gillaspie and Robert J. Webster III are with the Department of Medicine and Thoracic Surgery at the Vanderbilt University Medical Center, Nashville, TN 37212, USA.

[3]Alan Kuntz is with the Robotics Center and the Kahlert School of Computing at the University of Utah, Salt Lake City, UT 84112, USA.

Digital Object Identifier (DOI): see top of this page.

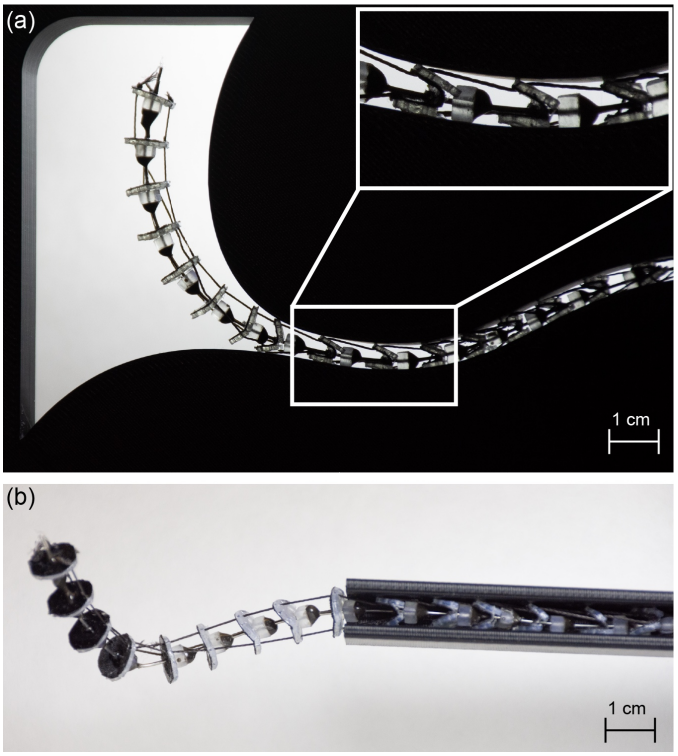

Fig. 2: A new tendon-driven robot with disks that collapse to squeeze through spaces narrower than their native cross-section. (a) demonstrates a straight tendon being pulled while (b) shows a helical tendon path creating a more complex, nonplanar shape.

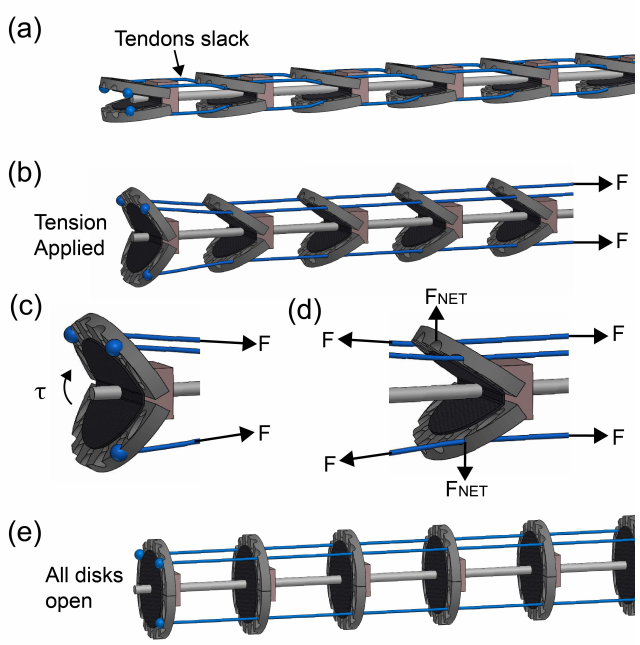

Fig. 3: Diagram showing the mechanism for passive unfolding of the disks. The half disks (grey) are attached by a thin layer of silk (black). Backstops are shown in pink and tendons in blue. (a) When the disks exit the port, they remain folded as tendons are slack. (b) Tension is applied to the tendons, applying a torque on the front disk about the hinge, causing it to open. As the tendons straighten to their nominal configuration, they exert outward force on the subsequent disks, opening them. (c) and (d) A free body diagram of the tendon forces which open the disks. (e) All disks open with tension.

through the openings between the ribs. Since continuum robots are actuated by elastically bending their backbone, they can navigate the workspace without pivoting and tilting about the insertion. In addition, the change in cross-sectional geometry enabled by the proposed folding mechanism results in smaller incisions that better conform to the narrow interstitial space between the ribs.

This folding concept was inspired by shape changing capabilities that have recently been integrated into a variety of soft robot morphologies for navigation in constrained spaces [13]. Mobile quadrupeds have been designed that can flatten to slide under obstacles that present a narrow, wide opening like the bottom of a closed door [14]. A vine-like robot that grows from its tip has been proposed that can squeeze through a variety of narrow openings [15]. Shape changing concepts have been integrated into continuum robots to adjust length and increase torsional stiffness [16], and tendon-actuated continuum robots that can adapt their length [17] and stiffness [18] have been proposed. Abah, et al., also proposed a variable geometry continuum robot that can alter its diameter through scissor linkages [19], though the mechanical complexity of this design may make it challenging to miniaturize for surgical applications.

This paper makes several contributions to continuum robotics. We introduce a new tendon-actuated continuum manipulator concept that can fold to squeeze through narrow openings. We propose designs that fold along one axis to flatten, and designs that fold along multiple axes to reduce their diameter. The multiple axis results in this paper consist of a brief summary of results initially published in preliminary conference form in [20]. Perhaps most importantly, we show experimentally that these designs behave kinematically similarly to traditional continuum robots at various deployment lengths.

II. Robot Concept

Our foldable robot concept consists of a central backbone augmented with foldable disks through which tendons pass (Fig. 3). Hard-stops affixed to the backbone support each disk during actuation. Each support disk has holes drilled around its periphery so that tendons can be routed through paths that are either linear or nonlinear when the robot is in its unactuated, straight configuration. To reduce the effects of friction when disks are folded, we altered the geometry of the holes through which the tendons pass. The new disks feature holes drilled both perpendicular to the disk (so that the hole runs parallel to the tendon when fully open), and at an angle (angled in the direction of folding) in order to align more closely with the tendon routing when the disks are folded. This concept is shown in Fig. 4c.

Our foldable disks are made from two rigid half-disks connected by a flexible material that acts as a living hinge and enables bending along the midline of the disk, as shown in Fig. 3. In traditional tendon-operated continuum robots, these support disks are usually affixed to the backbone and serve to constrain tendons along the robot. Since the folding nature of our disks makes it challenging to directly affix them to the

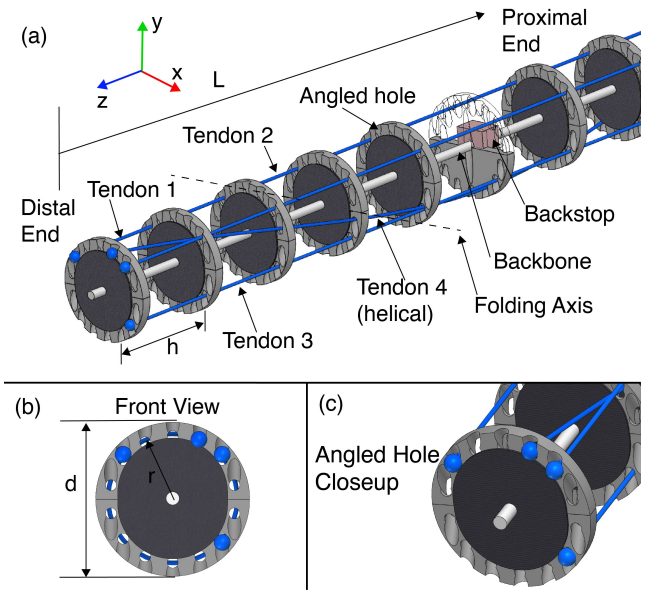

Fig. 4: Drawing showing the parameters and tendon routing strategy for the prototypes. The traditional version of this prototype is identical to the one shown except that its disks do not fold.

backbone, we instead include a hard stop behind each disk. Each hard stop is glued onto the backbone, constraining the disk axially, while preventing it from opening further than the plane perpendicular to the backbone. The back of each disk is keyed to fit the hard stop that is attached to the backbone, preventing axial rotation of the disk when open.

Typical tendon-actuated continuum robots route the tendons parallel along the robot's backbone. However, by employing arbitrary tendon routing strategies [10], we can beneficially modify the workspace and dexterity of the manipulator [10]–[12]. Fig. 1 (b) and Fig. 2 (b) demonstrate this complex routing concept.

III. Prototype and Experiments

To evaluate this new foldable tendon-actuated concept, we compare it directly to a standard tendon-actuated robot that has the same parameters as our prototype (length, disk size, spacing, tendon routing) but with disks that do not fold. We evaluate the workspaces of the two robots, a capability relevant for performing surgical tasks, as well as analyze the difference in tendon tension (which is the input for model predictions). The reason for these experiments is to determine whether a new kinematic model is needed for the folding robot or whether established models still apply [10].

A. Prototypes

We built two tendon-actuated prototypes for experimental evaluation, one with folding disks and one without. Each prototype is made using the routing strategy and parameters shown in Fig. 4 and listed in Table I. The disk spacing (h) was chosen according to the optimal ratio of 0.4 for disk spacing to tendon distance from backbone discussed in [21]. Silk fabric 0.4 mm thick is used as a living hinge connecting the two half disks. Silk has been used for other soft robot applications

TABLE I: Parameters used for each tendon actuated prototype.

Parameter	Value
Diameter (d)	14 mm
Hole Distance to Center (r)	5.5 mm
Disk Spacing (h)	13.5 mm
Total Length (L)	216 mm
Backbone OD	1.2 mm
Backbone ID	0.88 mm
Disk Thickness	1.0 mm

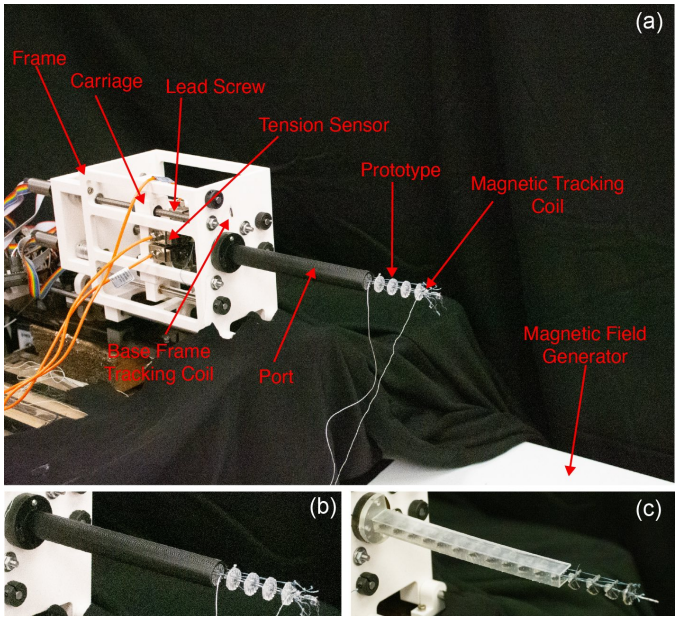

Fig. 5: Experimental setup. (a) The frame is fixed in place above the field generator using hot glue. 4 carriages with tension sensors pull the tendons for each prototype. The workspace measurements are taken using the tracking coils attached to the prototype, and one of the ports used to constrain the prototype is shown here. (b) shows the circular port used for the standard tendon drive robot and (c) shows the rectangular port used for the folding prototype. The ports displayed here cover 75% of the arc length.

due to its high tensile strength and ability to withstand cyclic loading [22], which is desirable for the hinges because it resists tearing while being flexible and inelastic (very little stretch). We note that this choice of material for the hinge means that the disks fold passively, and though the disks start in the folded configuration when coming out of the port, they will open when tension is applied to the tendons (see Fig. 3 for a demonstration of this concept).

The folding prototype is approximately 4 mm thick when folded, and each disk folds along the axes defined in Fig. 4 (each folding axis is parallel to the x-axis according to the coordinate frame, and folds toward the positive z-axis along the backbone). There are 14 holes drilled around the periphery of each disk to facilitate both curved tendon routing and multiple straight tendons (shown Fig. 4), just as was done in the prototype in [10].

For this initial prototype, we use a hard resin (Clear, Formlabs, Inc.) to make the rigid half-disks, and silk fabric, as mentioned earlier, to create the living hinge. The fabric is glued to two half-disks to connect them, making a solid cir-

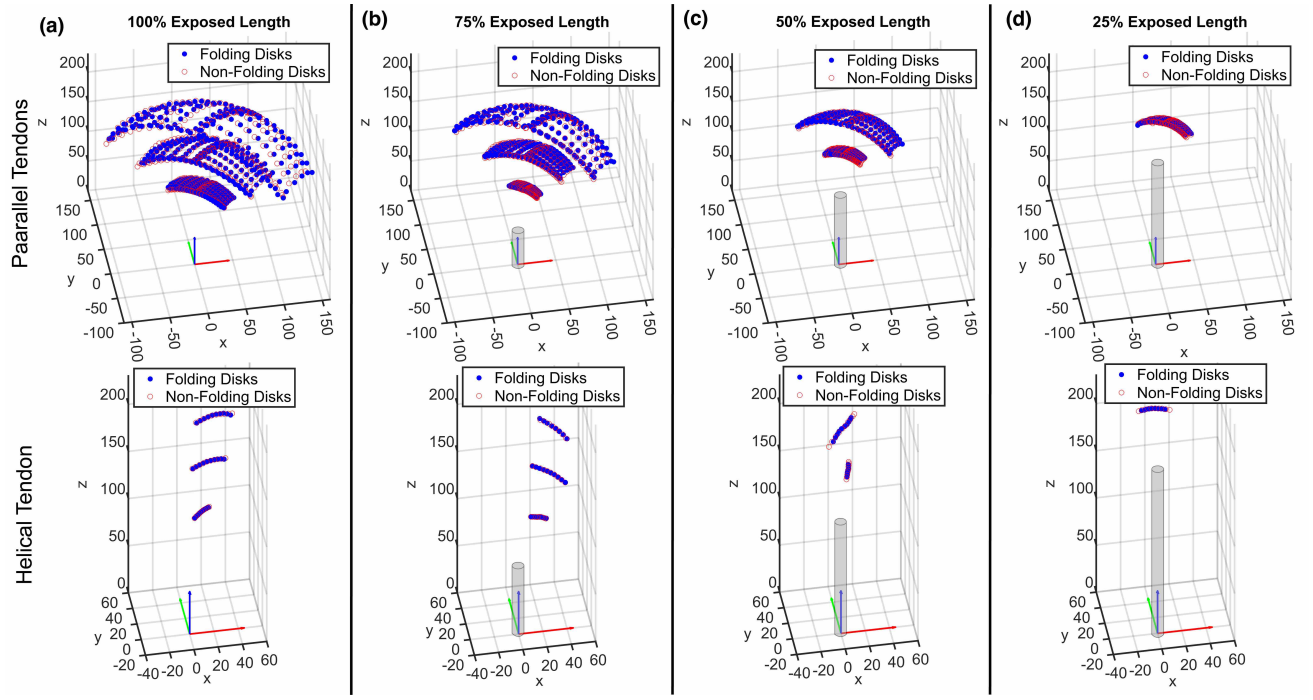

Fig. 6: Workspaces for the folding and non-folding robot prototypes at 4 different deployment lengths ((a) 216 mm, (b) 162 mm, (c) 108 mm, and (d) 54 mm). The robot was actuated using three parallel routed tendons (top) and one helical (bottom) to sweep through different configurations. The prototype with folding disks is shown in blue, and the prototype with non-folding disks is in red, with a representative port shown in gray.

cular shape when unfolded, and two half circles when folded. The hard stop that prevents translation and rotation is also 3D printed from the same resin, and is attached to the backbone using epoxy (Henkel Loctite EA 9460). A small amount of epoxy is also placed on the backbone in front of each disk to prevent forward translation while still enabling folding. The tendons are made from a braided polyethylene, which has high tensile strength, low friction, and is approximately inextensible.

B. Experimental Setup

We built an actuation unit for these experiments that consists of four carriages that can be independently translated to pull the tendons. Each carriage is attached to a lead screw and a linear translation rod to prevent rotation. The lead screws are actuated by Maxon motors and controlled by EPOS4 modules (Maxon Precision Motors, Inc.). The four carriages are contained within a 3D printed frame that in future work could be translated to insert and retract the robots. The ports used to constrain the prototypes are also 3D printed, shown in Fig. 5 (b) and (c). Prior to deployment, the folding mechanism is loaded into the rectangular port outside of the body. Then, the insertion degree of freedom will push the folding robot through the rectangular port, and they will naturally open as they leave the port constraint, fully opening once tension is applied. During retraction, the edge of the port pushes the disks back into their closed configuration. This can also be seen with the multi-plane folding design in Fig. 8.

To measure the workspace, we used magnetic tracking coils (Northern Digital Inc., Canada) fixed to the backbone. Each prototype had three 6DOF sensors attached - one at the tip (100% arc length), one at 75% arc length, and one at 50% arc length. A fourth sensor was placed on the front plate to provide a reference location between the two prototypes. The experimental setup is shown in Fig. 5.

Additionally, each carriage was equipped with a load cell with a 50 kg capacity to measure tendon tension throughout actuation. The tension was not used to control tip movement during these experiments, but to measure differences in tendon tension between the folding and traditional prototype. Prior to the experiments, we probed equidistant points around the backbone using a tracking probe in order to calibrate the base frame of the robot to the tracking system coordinate frame. The magnetic tracking coils recorded absolute position of the backbone throughout the experiments in using the field generator's global coordinate system. Additionally, we calibrated the frames between the two prototypes in post-processing using a rigid transform, which helped account for any errors in alignment when placing the tracking coils on the backbone.

C. Kinematics Experiment

In this section, we explore the kinematics of each prototype for different deployment lengths and tendon configurations. In these experiments, we used straight tendons and helically routed tendons and examine the shape at various insertion arc lengths. We show that the two prototypes cover nearly the same kinematics for the same tendon displacements. As expected, tendon tensions are higher in the folding prototype due to tendon interactions with folded disks where it passes through the constraint, as discussed in the next section.

TABLE II: Difference in position between the two prototypes for the kinematics experiments. The results shown represent the error (assuming the standard prototype is ground truth), standard deviation, and error as a percentage of arc length for each sensor for both the parallel routed and helically routed tendons. Error at the 50% arc length sensor and 75% arc length are not displayed for cases where those sensors were covered by the port.

	100% Exposed Length			**75% Exposed Length**			**50% Exposed Length**			**25% Exposed Length**		
	Mean Error (mm)	Std. Dev. (mm)	% Arc Length Error	Mean Error (mm)	Std. Dev. (mm)	% Arc Length Error	Mean Error (mm)	Std. Dev. (mm)	% Arc Length Error	Mean Error (mm)	Std. Dev. (mm)	% Arc Length Error
Parallel Tendons												
Tip Sensor	5.05	2.69	2.34%	3.80	2.69	2.35%	3.95	2.69	3.66%	3.26	1.89	6.04%
75% Arc Length Sensor	3.42	2.09	2.11%	2.84	1.45	2.63%	2.53	1.25	4.69%	N/A	N/A	N/A
50% Arc Length Sensor	1.55	0.78	1.44%	1.39	0.64	2.57%	N/A	N/A	N/A	N/A	N/A	N/A
Helical Tendon												
Tip Sensor	0.86	0.55	0.40%	0.88	0.38	0.54%	3.02	1.92	2.80%	1.50	1.15	2.78%
75% Arc Length Sensor	0.62	0.45	0.38%	0.43	0.18	0.40%	1.68	0.92	3.11%	N/A	N/A	N/A
50% Arc Length Sensor	0.52	0.33	0.48%	0.35	0.18	0.65%	N/A	N/A	N/A	N/A	N/A	N/A

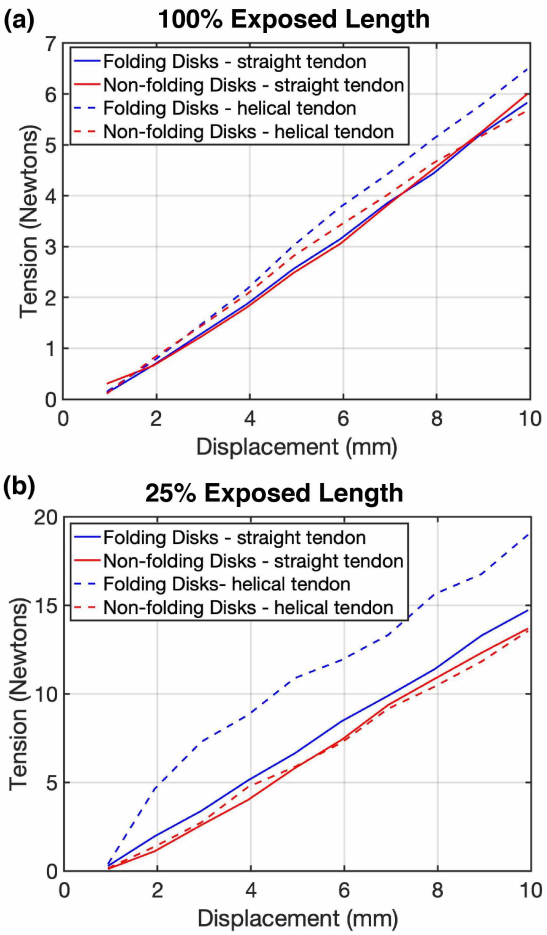

Fig. 7: Tension vs displacement during the workspace experiments shown for two cases - 100% exposed length and 25% exposed length. One straight and one helically routed tendon are shown.

We performed two experiments to test the kinematics of each prototype—the actuation of 3 straight tendons to show a wide sweep of the workspace and the actuation of 1 helically routed tendon to demonstrate the use of complex tendon routings with this design. The exact routing locations for each tendon are shown in Fig. 4, and were chosen somewhat arbitrarily, though future work could include optimization of the tendon routing to achieve a particular goal. The configuration space was defined as displacements of each tendon at linearly spaced intervals of 2mm from [0-10mm], sweeping through all permutations of straight tendon displacements. The helically routed tendon was actuated separately for these experiments.

We acquired data at a variety of insertion arc lengths using rigid ports (see Fig. 5 for example). The traditional prototype was constrained by ports 1 mm larger than its circular cross section, making them 15 mm in diameter. For the folding prototype, we reduced this dimension by half in one direction, making the ports rectangular in shape with a cross section of 7.5 mm by 15 mm. Since the disk's folding mechanism is passive, it may remain partially folded, even when deployed, until tendons are pulled taut and force the disks open. Prior to collecting data for a particular tendon, we pre-tensioned that tendon by pulling it to the point just before backbone movement occurred. We allowed the tendon on the outside of the curvature arc to remain slack, and due to the nature of the passive folding, allowed the outside disk to remain partially folded. However, the disk would reopen when tension was applied to the outside tendon. For both manipulators, the insertion arc lengths used were 100% (216 mm length), 75% (162 mm length), 50% (108 mm length), and 25% (54 mm length) of the total arc length of the manipulator.

Fig. 6 compares the kinematics of the two prototypes for the straight (parallel) and helical tendon configurations, illustrating the similarity between the two. Examples of a physical prototype being actuated by a straight tendon and a helical tendon can be seen in Fig. 2. The numerical results for each are also shown in Table II, where we can see that the mean error for the folding prototype remains low in all configurations. The highest error occurs at the 25% exposed length case, where we can see error as a percentage of arc length is 6.04% for the straight tendon and 2.78% for the helical tendon at the tip. We know from [10] that the highest model error occurs at the highest tensions, which may account for the increase in error as more of the disks are folded within the port. Since we were actuating the disks with equivalent displacement and not tension, we hypothesize that the folded disks increased the tension in the tendons, leading to higher errors when compared to the standard tendon driven prototype, which we begin to explore in the next section.

We also quantify the change in workspace size between the folding and non-folding prototypes. For each of the insertion cases shown in the top row of Fig 6, we compute an estimate

for the workspace size by projecting the tip position into the xy plane, and then computing the area of the convex hull for each set of points. The area of the workspaces shown in the top row of Fig. 6 are summarized in Table III. We note that for all the insertion lengths, the change in the workspace size is less than 12%, which we believe is not a significant difference for practical purposes. We believe these differences can be attributed to fabrication error, as well as sensor placement error between prototypes.

TABLE III: Comparison of Workspace Size

Exposed Length	Workspace Area (cm^2)	
	Folding Design	Non-folding Design
100 %	312	305
75 %	191	180
50 %	78	75
25 %	17	19

D. Tendon Tension

Here we explore the differences in the tendon tension between the folding prototype and the traditional prototype. An average tension was measured at each carriage configuration, and for each experiment with both the folding and the non-folding prototypes. Two example cases are shown here - each prototype with the full arc length exposed, and each prototype with 25% of its arc length exposed. We can see that in the case of the non-folding prototype (conventional tendon-actuated robot, as seen in previous literature), the tendon tension is linearly related to the distance the carriage moved (see Fig 7). One can also see that the tension for a straight tendon and a helically routed tendon is nearly identical throughout the tendon displacements. This still holds true for the folding prototype at 100% arc length exposed (i.e., no disks folded and thus introducing additional frictional effects), shown in Fig. 7a.

The 25% arc length is the worst-case scenario for these experiments where the most disks are folded, which is where we would expect to see the greatest increase in friction. We can see in Fig. 7b that tension increases for the folding prototype when its disks are folded in the case of the helically routed tendon. The straight tendon with folded disks performs very similarly to the traditional prototype, although there is a slight increase in tension for this prototype.

Though more testing is needed, we anticipate that for many cases, the new, folding disk prototype will adhere well to the conventional model stated in [10].

IV. Extension to Multi-plane Folding

The first design presented in this work demonstrates how single-plane folding disks can be used to enter workspaces with dimension constraints in a single direction, such as the rib cage. In other applications, one may wish to reduce the total diameter of the device, which would require folding in multiple directions. To explore the feasibility of this we constructed the following prototype. This diameter-changing

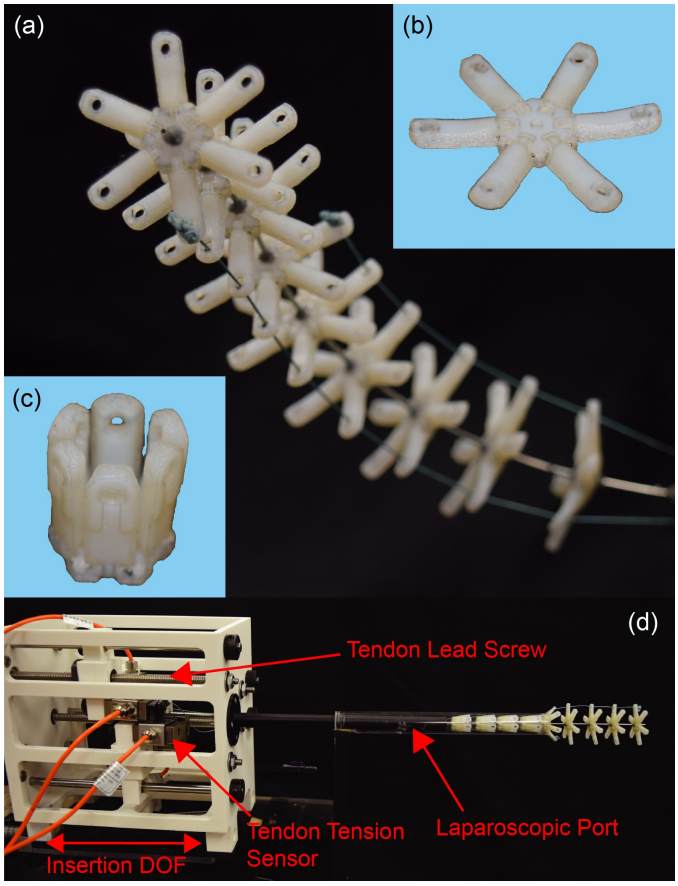

Fig. 8: Conceptual mechanism design of a multi-plane folding tendon robot and deployment system.

manipulator prototype consists of a central hollow elastic backbone with support "disks", each consisting of a hub with 6 folding arms. The arms and central hub were 3D printed from ABS-like resin (Stratasys: printer J35, resin RGD-531/515). Folding is constrained with 0.72 mm diameter steel pins which provide more rigidity for the much smaller folding crease as compared to the living hinge design. To enable passive opening of the arms after passing through the port, laser-cut rubber backing 0.4 mm thick was secured to the back of each disk with Loctite adhesive. The rubber is stretched in the folded configuration, causing the arms to naturally extend when port constraints no longer hold them closed. Figure 8(a) shows this multi-plane folding concept, and insets (b) and (c) demonstrate the pin-hinge folding mechanism. Figure 8(d) demonstrates how the multi-plane folding prototype can be introduced into the workspace through a port; The laparoscopic port (clear) is envisioned to be fixed relative to the patient, while the insertion DOF on the tendon carrier introduces the folding mechanism through the port, allowing the support disks to passively unfold once they enter the workspace.

To validate the kinematics of the multi-plane folding design, we inserted a fiber bragg shape sensor (*Pathfinder-Lab: The Shape Sensing Company*) into the inner lumen of the nitinol backbone to measure the full shape. We tested a single tendon terminating at the tip of the device pulled at a range of tensions, and compared the full shape to the Cosserat tendon

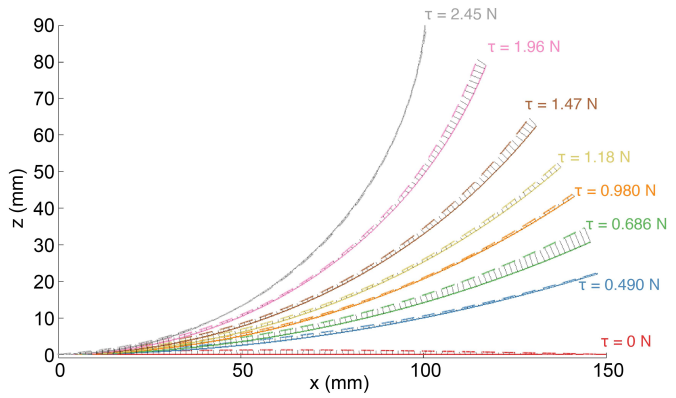

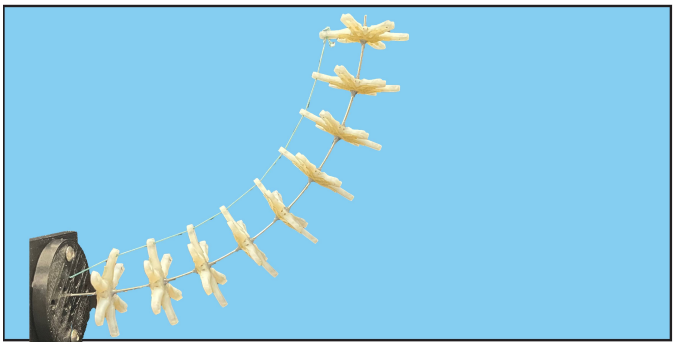

Fig. 9: Kinematic model evaluation of multiplane folding concept.

robot model proposed in [10]. Figure 9 shows the measured (dashed) and model-predicted (solid) backbone shape; the experimental setup is shown in Fig. 8(d).

V. Impact of Partial Disk Folding on Compliance and Tendon Routing

In this section we provide a theoretical analysis of the effect of disk folding on the performance of the manipulators. Since the disks passively open, as long as there is tension in the tendons, the terminating force of each tendon on the last distal disk will cause it to fully unfold. However, there is a chance that in certain configurations the remaining disks will not fully unfold due to external loads or other factors. This will cause the tendon routing paths with respect to the backbone to change, which will affect the distributed forces and moments imparted by each tendon on the central backbone. If one knows how much the disk is folded (by encoders, cameras, or other means) one can compute the position of the tendon in the robot's cross section and use the model proposed in [10] to determine the robot's shape. This model assumes that there is no cross-sectional deformation and that the tendon routings are constant in the local rod frame. Writing the position of tendon routing $(x_t,\, y_t)$ in terms of the radius r from the backbone and angle ψ as in [12], and assuming that the folding disks are partially unfolded by an angle γ (see Fig. 10) relative to their nominal configuration, the new location of the tendon is:

$$\begin{aligned} x_t' &= r\cos\gamma\cos\psi \\ y_t' &= r\sin\psi \end{aligned} \tag{1}$$

The multi-arm folding design is radially symmetric, and the

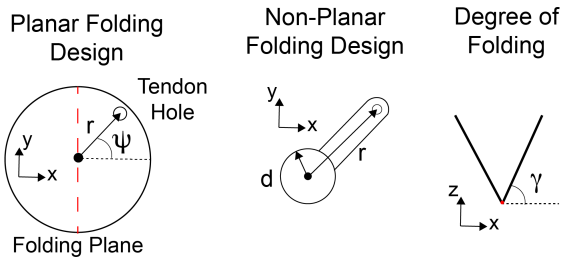

Fig. 10: Diagram demonstrating the relevant parameters in the kinematic model that change with partial folding for each design.

folding joint is located at an offset d from the backbone. Therefore the new location of the tendon routing is:

$$\begin{aligned} x_{tr}' &= [d(1-\cos\gamma) + r\cos\gamma]\cos\psi \\ y_{tr}' &= [d(1-\cos\gamma) + r\cos\gamma]\sin\psi. \end{aligned} \tag{2}$$

The radially folding design only decreases the radial hole offset as the disks partially fold, thus one would expect the magnitude of curvature to decrease slightly, while the direction would remain unchanged. In contrast, the half-folding design only changes the position of the tendon in a single direction (x); this causes the effective angle of the tendon path to change; this will cause both magnitude and direction of curvature to change slightly.

The compliance of tendon robots with linear tendons to external loads is explored in [23]. Modelling the backbone as an Euler-Bernoulli beam, we can use the constitutive stiffness law (3). The internal moment of the backbone assuming a straight routed tendon and an external force applied at the tip then (4):

$$m(s)ds = -EId\theta \tag{3}$$

$$m(s) = (s-L)F + r(s)\tau, \tag{4}$$

where $r(s)$ is the tendon offset from the backbone, which can be calculated from (1) or (2) based on the measured hinge angle, and F is an external force applied at the tip. Integrating (4) to solve for the bending angle $\theta(s)$:

$$\theta(s) = \frac{-1}{EI}\left[\frac{1}{2}Fs^2 - FLs + \tau\int_0^L r(s)ds\right], \tag{5}$$

where the tendon tension $\tau = k\Delta$, which is the product of tendon stiffness and stretch, can be calculated using

$$\Delta = \int_0^L r(s)\left(\frac{\mathrm{d}\theta}{\mathrm{d}s}\right)\mathrm{d}s. \tag{6}$$

The bending angle $\theta(s)$ can then be integrated once more to solve for the deflection of the backbone. The analytical solution for tip deflection from an applied tip force for a tendon with linearly varying radius is derived in [23]. If the angle of disk opening is known, for example from an encoder or via visual feedback or other sensing, it would be possible to use the equations presented here to predict the shape and response to external loads of the tendon robot using the model proposed in [10].

VI. Conclusion

In this paper, we presented a new concept enabling continuum robots to change their dimensions to reduce diameter and navigate through narrow openings, inspired by the medical motivation of fitting between the ribs for minimally invasive lung surgery. We make this possible by employing folding disks via a passive hinge. We demonstrated that this robot can be deployed through a port with a smaller cross-section than the robot's nominal diameter, and that it can be effectively actuated beyond the insertion constraint. The robot's kinematics were found to be comparable to an equivalently made traditional continuum robot whose disks do not fold. This implies that prior modeling and control approaches should directly apply to these new folding robots, though we explore the possibility of failure to open and the effects on the kinematic model. Future work could investigate a model that accounts for the interaction between the coupled interaction between hinge elasticity and the tendon loads and manipulator shape. The one trade-off we observed for folding is an increase in tendon tension when the robot is constrained through a narrow opening, due to increased frictional effects between the tendons and disks. However, these effects were not noticeable until they accumulated over many disks (when very few disks were outside of the port).

We aim to continue developing the folding robot concept into a functional, multi-arm continuum robot system for minimally invasive lung surgery, as envisioned in Figure 1. Based on the forward kinematic model proposed in [10], we will develop a resolved rates controller for a folding tendon robot with four actuated tendons and an insertion degree of freedom through the laparoscopic port. An interesting area of future work could be to investigate the dynamic effects of the folding mechanism, including any dissipative damping caused by the living hinge folding mechanism, as well as considering both passive and active unfolding mechanisms. We will also explore the effects of these new design parameters on stiffness and the range of achievable curvature. Towards the intended use case of lung surgery, we aim to quantify the workspace and force requirements for a VATS wedge resection procedure, and then design the geometric parameters of the folding robot, including the routing of tendons, length, and diameter based on the method described in [12]. More complex tendon routing will be employed in future designs to enable orientation control of the robot. Following the construction of these task specific manipulators, we will develop a retractor, gripper, and cutting tool to be integrated with the tendon manipulators.

We believe that the design proposed in this paper enables continuum robots enter highly constrained environments with the ability to alter their cross-section. The new folding concept proposed in this work shows promise for highly dexterous, minimally invasive thoracoscopic surgical tools.

References

[1] "Lung Cancer Statistics — How Common is Lung Cancer?" [Online]. Available: https://www.cancer.org/cancer/lung-cancer/about/key-statistics.html

[2] D. Kim and J. W. Lee, "Current Status of Lung Cancer and Surgery Based on Studies Using a Nationwide Database," *Journal of Chest Surgery*, vol. 55, no. 1, p. 1, 2 2022.

[3] M. K. Gould, J. Donington, W. R. Lynch, P. J. Mazzone, D. E. Midthun, D. P. Naidich, and R. S. Wiener, "Evaluation of individuals with pulmonary nodules: When is it lung cancer? Diagnosis and management of lung cancer, 3rd ed: American college of chest physicians evidence-based clinical practice guidelines," *Chest*, vol. 143, no. 5 SUPPL, pp. e93S–e120S, 5 2013.

[4] M. Bendixen, O. D. Jørgensen, C. Kronborg, C. Andersen, and P. B. Licht, "Postoperative pain and quality of life after lobectomy via video-assisted thoracoscopic surgery or anterolateral thoracotomy for early stage lung cancer: a randomised controlled trial," *The Lancet. Oncology*, vol. 17, no. 6, pp. 836–844, 6 2016.

[5] J. M. Reinersman, E. Passera, and G. Rocco, "Overview of uniportal video-assisted thoracic surgery (VATS): Past and present," *Annals of Cardiothoracic Surgery*, vol. 5, no. 2, pp. 112–117, 2016.

[6] T. Homma, Y. Doki, Y. Yamamoto, T. Ojima, Y. Shimada, N. Kitamura, and N. Yoshimura, "Risk factors of neuropathic pain after thoracic surgery," *Journal of thoracic disease*, vol. 10, no. 5, pp. 2898–2907, 2018.

[7] I. D. Walker, "Continuous backbone "continuum" robot manipulators," *ISRN Robotics*, vol. 2013, p. 726506, 2013.

[8] R. J. Webster and B. A. Jones, "Design and kinematic modeling of constant curvature continuum robots: A review," *The International Journal of Robotics Research*, vol. 29, no. 13, p. 1661–1683, Nov 2010.

[9] J. Burgner-Kahrs, D. C. Rucker, and H. Choset, "Continuum robots for medical applications: A survey," *IEEE Transactions on Robotics*, vol. 31, no. 6, p. 1261–1280, 2015.

[10] D. C. Rucker and R. J. W. III, "Statics and dynamics of continuum robots with general tendon routing and external loading," *IEEE Transactions on Robotics*, vol. 27, no. 6, p. 1033–1044, 2011.

[11] J. Starke, E. Amanov, M. T. Chikhaoui, and J. Burgner-Kahrs, "On the merits of helical tendon routing in continuum robots," in *IEEE/RSJ International Conference on Intelligent Robots and Systems*, 2017, pp. 6470–6476.

[12] M. Rox, A. Copinga, R. P. Naftel, R. J. Webster III, and A. Kuntz, "Optimizing Continuum Robot Tendon Routing for Minimally Invasive Brain Surgery," in *Hamlyn Symposium on Medical Robotics*, 2022.

[13] D. Shah, B. Yang, S. Kriegman, M. Levin, J. Bongard, and R. Kramer-Bottiglio, "Shape Changing Robots: Bioinspiration, Simulation, and Physical Realization," *Advanced Materials*, vol. 2002882, pp. 1–12, 2020.

[14] R. F. Shepherd, F. Ilievski, W. Choi, S. A. Morin, A. A. Stokes, A. D. Mazzeo, X. Chen, M. Wang, and G. M. Whitesides, "Multigait soft robot," *Proceedings of the National Academy of Sciences of the United States of America*, vol. 108, no. 51, p. 20400–20403, 2011.

[15] E. W. Hawkes, L. H. Blumenschein, J. D. Greer, and A. M. Okamura, "A soft robot that navigates its environment through growth," *Science Robotics*, vol. 2, no. 8, 2017.

[16] J. Santoso and C. D. Onal, "An origami continuum robot capable of precise motion through torsionally stiff body and smooth inverse kinematics," *Soft Robotics*, 2020.

[17] E. Amanov, T.-D. Nguyen, and J. Burgner-Kahrs, "Tendon-driven continuum robots with extensible sections—a model-based evaluation of path-following motions," *The International Journal of Robotics Research*, p. 0278364919886047, 2019.

[18] F. Maghooa, A. Stilli, Y. Noh, K. Althoefer, and H. A. Wurdemann, "Tendon and pressure actuation for a bio-inspired manipulator based on an antagonistic principle," in *IEEE International Conference on Robotics and Automation*, 2015, p. 2556–2561.

[19] C. Abah, A. L. Orekhov, and N. Simaan, "Design Considerations and Redundancy Resolution for Variable Geometry Continuum Robots," *Proceedings - IEEE International Conference on Robotics and Automation*, pp. 767–774, 9 2018.

[20] M. E. Smith, D. S. Esser, M. Rox, A. Kuntz, and R. J. Webster III, "A Radially Folding Mechanism to Enable Surgical Manipulators to Fit Through Smaller Ports," in *International Symposium for Medical Robotics*, 2023.

[21] C. Li and C. D. Rahn, "Design of continuous backbone, cable-driven robots," *Journal of Mechanical Design*, vol. 124, no. 2, p. 265–271, 2002.

[22] J. Xiong, J. Chen, and P. S. Lee, "Functional fibers and fabrics for soft robotics, wearables, and human–robot interface," *Advanced materials.*, vol. 33, no. 19, 2021-05.

[23] K. Oliver-Butler, J. Till, and C. Rucker, "Continuum robot stiffness under external loads and prescribed tendon displacements," *IEEE transactions on robotics*, vol. 35, no. 2, pp. 403–419, 2019.